ACS Photonics

Article

pubs.acs.org/journal/apchd5

Robustness of the Rabi Splitting under Nonlocal Corrections in Plexcitonics

Christos Tserkezis,*[,†] Martijn Wubs,*[,†,‡] and N. Asger Mortensen*[,§,‡]

[†]Department of Photonics Engineering and [‡]Center for Nanostructured Graphene, Technical University of Denmark, Ørsteds Plads 343, DK-2800 Kgs. Lyngby, Denmark

[§]Center for Nano Optics & Danish Institute for Advanced Study, University of Southern Denmark, Campusvej 55, DK-5230 Odense M, Denmark

ABSTRACT: We explore theoretically how nonlocal corrections in the description of a metal affect the strong coupling between excitons and plasmons in typical examples where nonlocal effects are anticipated to be strong, namely, small metallic nanoparticles, thin metallic nanoshells, or dimers with narrow separations, either coated with or encapsulating an excitonic layer. Through detailed simulations based on the generalized nonlocal optical response theory, which simultaneously accounts both for modal shifts due to screening and for surface-enhanced Landau damping, we show that, contrary to expectations, the influence of nonlocality is rather limited, as in most occasions the width of the Rabi splitting remains largely unaffected and the two hybrid modes are well distinguishable. We discuss how this behavior can be understood in view of the popular coupled-harmonic-oscillator model, while we also provide analytic solutions based on Mie theory to describe the hybrid modes in the case of matryoshka-like single nanoparticles. Our analysis provides an answer to a so far open question, that of the influence of nonlocality on strong coupling, and is expected to facilitate the design and study of plexcitonic architectures with ultrafine geometrical details.

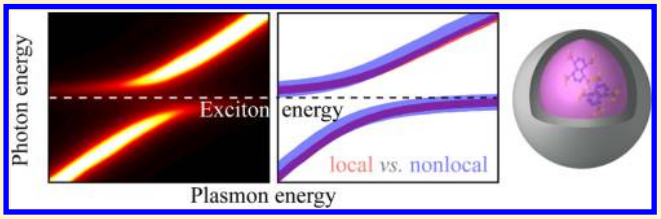

KEYWORDS: *plexcitonics, strong coupling, nonlocal optical response, Landau damping*

The strong coupling of excitons in organic molecules and quantum dots with surface plasmons has been attracting increasing interest in recent years.[1,2] Both propagating surface plasmons in thin metallic films[3−9] or localized surface plasmons in metallic nanoparticles[10−16] have been explored, not only from the point of view of theory, for which it constitutes a new class of light−matter interactions characterized by unique, hybrid optical modes,[17−21] but also because of its technological prospects in quantum optics and the emerging field of quantum plasmonics[22,23] as well as the design of novel optical components.[24−28]

Originally, strong coupling effects were studied for atomic and solid-state systems inside optical or photonic cavities.[29−32] *J*-Aggregates of organic molecules are however increasingly more frequently preferred, as they are characterized by large dipole moments and narrow transition lines.[11,33] At the same time, plasmonic architectures are excellent templates as cavities for the experimental realization of hybrid exciton−photon systems, because they provide nanoscale confinement and small modal volumes,[34] thus permitting even single-molecule strong coupling at room temperature.[35,36] The interaction of excitons with plasmons is usually traced through the Rabi splitting in optical spectra,[4,11] but recent elaborate experiments showed that it is also possible to observe the coherent energy exchange between the optical states of the two components in real time through the corresponding Rabi oscillations.[37−39] Tailoring the plasmonic environment is gradually departing from the regime of single nanoparticles,[12,13,40,41] and dimers[42−48] or nanoparticle arrays[49−53] are exploited to benefit from their stronger field confinement and enhancement. A similar coupling has also been observed for the interaction of emitters with the phononic modes of SiC antennae,[54] while engineering the electromagnetic vacuum through evanescent plasmon modes was recently proposed as a promising route toward increased light−matter interactions.[55]

As novel plasmonic architectures are explored in the quest for stronger, possibly even ultrastrong coupling,[56−58] reducing characteristic lengths such as nanoparticle sizes and/or separations is a natural step that goes hand-in-hand with advances in nanofabrication. In such systems, however, the excitation of a richness of hybrid optical modes characterized by large field intensities[59,60] is accompanied by the increased influence of nonclassical effects that require a description beyond classical electrodynamics.[61] Nonlocal screening due to the spatial dispersion of induced charges,[62−65] enhanced Landau damping near the metal surface,[66−68] electron spill-out,[69−74] and quantum tunneling[75−77] are different manifestations of the quantum-mechanical nature of plasmonic nanostructures in the few-nanometer regime, which need to

Special Issue: Strong Coupling of Molecules to Cavities

Received: May 29, 2017
Published: August 11, 2017

DOI: 10.1021/acsphotonics.7b00538
ACS Photonics 2018, 5, 133−142

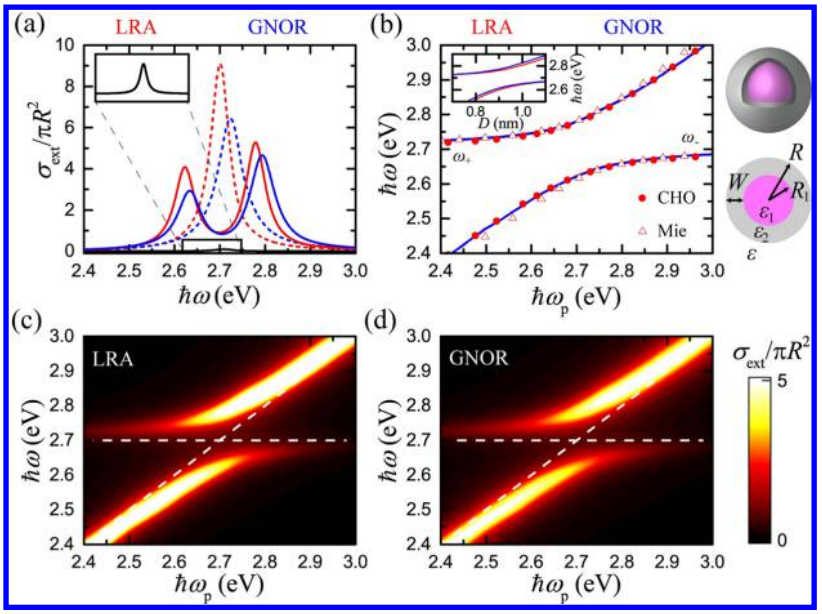

Figure 1. Strong coupling in the excitonic core−plasmonic shell nanoparticle shown in the schematics on the right. (a) Normalized extinction cross section (σ_{ext}) spectra in the absence (dashed lines) or presence (solid lines) of the excitonic core characterized by a transition at energy $\hbar\omega_{exc}$ = 2.7 eV, for a silver nanoshell with radius R = 5 nm and shell thickness W = 0.94 nm (for which the plasmon energy $\hbar\omega_p$ matches exactly $\hbar\omega_{exc}$). Red and blue lines represent LRA and GNOR results, respectively. The black line (magnified in the inset) shows the corresponding spectrum for a homogeneous excitonic sphere with R = 5 nm. (b) Extinction peaks of the two hybrid modes ($\omega_\pm$) as a function of $\hbar\omega_p$ within the LRA (red lines) and GNOR (blue lines) models. The plasmon energy is modified by changing the nanoshell thickness W and is calculated through the extinction peaks in the absence of an excitonic core for each model. Dispersion diagrams of the two modes directly as a function of W are shown in the inset. Red solid dots and open triangles denote the approximate solutions based on the CHO model and Mie-theory expansion, respectively, within LRA. Full extinction contour plots as a function of $\hbar\omega_p$ calculated with LRA and GNOR are shown in (c) and (d), respectively, sharing a common color scale. White dashed lines indicate the uncoupled exciton and plasmon energies.

be considered for an accurate evaluation of the emitter−plasmon coupling. For instance, nonlocal effects strongly affect spontaneous emission rates for quantum emitters in plasmonic environments[78] and lead to reduced near fields as compared to the common local-response approximation (LRA).[79] Fluorescence of molecules in the vicinity of single metallic nanoparticles[80] or inside plasmonic cavities[81] is also affected by a combination of nonlocal induced-charge screening and surface-enhanced Landau damping. In the context of strong coupling, Marinica et al. have reported quenching of the plexcitonic strength in dimers, attributed to quantum tunneling.[82] Even before entering the tunneling regime, one anticipates that experimentally observed nonlocal modal shifts and broadening[60,83,84] can manifest themselves as deviations in the dispersion diagram and changes in the width of the Rabi splitting in the optical spectra. Nevertheless, related studies are still missing, and these expectations are yet to be confirmed.

In the recent review by Törmä and Barnes,[1] one section was devoted to how smaller dimensions of the plasmon-supporting structures become increasingly more important. In particular, it was anticipated that *one consequence of nonlocal effects that is of great interest in the context of strong coupling is that of a reduction in the field enhancement that can be achieved when light is confined to truly nm dimensions*. Motivated by this discussion, and also by our recent studies of single emitters in plasmonic environments,[80,81] we explore here the influence of nonlocality on plexcitonics through theoretical calculations based on the generalized nonlocal optical response (GNOR) theory.[85] GNOR has proven particularly efficient in recent years in simultaneously describing both nonlocal screening and Landau damping through a relatively simple correction of the wave equation that is straightforward to implement to any plasmonic geometry model.[86] Here we take advantage of its flexibility to describe the optical response of typical plexcitonic architectures: metallic nanoshells either coated by an excitonic layer or containing it as nanoparticle core, dimers of such nanoshells, and homogeneous nanosphere dimers encapsulated in an excitonic matrix. In all situations it is shown that, while nonlocal modal shifts introduce a detuning for fixed geometrical details, the width of the Rabi splitting remains in practice unaffected if one follows the more practical approach of modifying nanoparticle sizes and/or separations so as to tune the plasmon mode to the exciton energy. Broadening of the plasmon modes due to Landau damping is also shown to be weak enough, so as to ensure that the two hybrid modes remain distinguishable and line-width-based criteria for strong coupling are satisfied. This somehow unexpected result is interpreted in view of a popular coupled-harmonic-oscillator (CHO) model and the strength of the coupling as related to the modal volume, while analytic solutions for the hybrid modes are obtained based on Mie theory. Our analysis reduces concerns about nonlocal effects in the coupling of plasmons with excitons and provides additional flexibility to the experimental realization of novel plexcitonic architectures with sizes in the few-nanometer regime.

RESULTS AND DISCUSSION

In order to facilitate a strong influence of nonlocality, we consider throughout this paper small nanoparticles with radii that do not exceed 20 nm and thin metallic shells of 1−2 nm width. While such thin nanoshells are still experimentally challenging, successful steps toward this direction have been presented recently.[87] The choice of nanoshells over homogeneous metallic spheres serves a dual purpose. On one hand,

DOI: 10.1021/acsphotonics.7b00538
ACS Photonics 2018, 5, 133−142

thin metallic layers ensure the reduced lengths required for a strong nonlocal optical response, even though the far-field footprint of nonlocality can often prove negligible.[88,89] On the other hand, and more importantly, modifying the shell thickness provides the required plasmon tuning[90] to match the exciton energy and observe the anticrossing of the two hybrid modes in dispersion diagrams.[12,58] As discussed by Törmä and Barnes,[1] metals with low loss are beneficial for strong-coupling applications, because the plasmon modes should have line widths comparable to those of the excitonic material. In our case, low intrinsic loss also ensures that the role of Landau damping will be better illustrated. For this reason, silver is adopted as the metallic material throughout the paper.

As a first example of a nonlocal plexcitonic system, we study a silver nanoshell of total radius R = 5 nm in air, encapsulating an organic-dye core of variable radius R_1, so that the metal thickness is $W = R - R_1$, as shown in the schematics of Figure 1. The dye is modeled as a homogeneous excitonic layer with a Drude−Lorentz dielectric function as described in the Methods section, with its transition energy at $\hbar\omega_{exc}$ = 2.7 eV. The extinction (σ_{ext}) spectrum for a homogeneous sphere of radius R = 5 nm described by such a permittivity is shown in Figure 1a by the black line (magnified in the inset) and is indeed characterized by a weak resonance at 2.7 eV. A red (blue) dashed line depicts the corresponding LRA (GNOR) extinction spectrum for a hollow silver nanoshell (in the absence of the excitonic core) with R = 5 nm and W = 0.94 nm, the thickness for which the symmetric particle-like plasmon mode of the nanoshell[91] matches $\hbar\omega_{exc}$ in the local description. As expected, when nonlocal effects are taken into account through GNOR, for the same geometrical parameters the plasmon mode experiences both a blue-shift, of about 0.023 eV, and additional broadening, so that the full width at half-maximum of the resonance increases from 0.05 eV to 0.067 eV. Once the dye core is included, its excitonic mode interacts with the localized surface plasmon, and two hybrid modes are formed, as shown by solid red and blue lines in Figure 1a, with a Rabi splitting of energy $\hbar\Omega_R$ = 0.156 eV. While both peaks experience a nonlocal blue-shift, its strength is practically the same, so that $\hbar\Omega_R$ remains unaffected. However, one should be cautious and not draw conclusions just from Figure 1a, since the spectra have been calculated for a shell thickness for which the plasmon mode is detuned from $\hbar\omega_{exc}$ in the nonlocal description.

In order to get a better visualization of the strong coupling of Figure 1a, we plot in Figure 1b the dispersion diagram of the two modes as a function of the plasmon energy $\hbar\omega_p$, calculated by modifying the shell thickness and obtaining the resonance peak for hollow nanoshells. We then repeat the calculation in the presence of the dye and obtain the frequencies of the hybrid modes, $\omega_\pm$, from the extinction spectra. Plotting the energies of the two hybrid modes as a function of $\hbar\omega_p$ leads to dispersion lines that are practically indistinguishable for the LRA (red lines) and GNOR (blue lines) models. The same dispersion diagram is plotted in the inset of Figure 1b as a function of shell thickness. It is straightforward to see that the GNOR dispersion lines are just horizontally shifted with respect to the corresponding LRA ones, as the nonlocal blue-shift makes thicker shells necessary to achieve the same plasmon energy.

Together with the numerical results, in Figure 1b we also present the solutions obtained through two different analytic approaches: solid red circles represent the hybrid mode frequencies obtained from the CHO model, while open triangles correspond to analytic solutions based on Mie theory; both are in excellent agreement with the full simulations. Due to its simplicity, the oscillator model is frequently adopted in the literature to describe the modes in strongly coupled plexcitonic geometries.[7,42,45] In the general case, the (complex) energies of the two hybrid modes are given by[1,16]

$$\hbar\omega_\pm = \frac{\hbar\omega_p + \hbar\omega_{exc}}{2} - i\frac{\hbar\gamma_{exc}}{4} - i\frac{\hbar\gamma_p}{4} \pm \frac{1}{2}\sqrt{(\hbar\Omega_R)^2 + \left[(\hbar\omega_p - \hbar\omega_{exc}) + i\left(\frac{\hbar\gamma_{exc}}{2} - \frac{\hbar\gamma_p}{2}\right)\right]^2} \quad (1)$$

where γ_p and γ_{exc} are the uncoupled plasmon and exciton damping rates, respectively. The frequency of the Rabi splitting is usually obtained by the simulated or experimental spectra at the crossing point, and it is directly related to the coupling strength g through $\hbar\Omega_R = 2g$. When absorptive losses are low and the plasmon and exciton line widths are similar, eq 1 simplifies to[92]

$$\hbar\omega_\pm = \frac{\hbar\omega_p + \hbar\omega_{exc}}{2} \pm \frac{1}{2}\sqrt{(\hbar\Omega_R)^2 + (\hbar\omega_p - \hbar\omega_{exc})^2} \quad (2)$$

We note here that, since the width of the Rabi splitting is itself often obtained from the dispersion diagrams, instead of more elaborate, quantum-mechanical analyses based on the coupling strength, it is not that surprising that eq 2 reproduces the same data so well. On the other hand, for spherical particles one can obtain the position of the modes through the poles of the scattering matrix in the Mie solution,[81] an approach that is the nanoparticle equivalent to introducing the metal and excitonic dielectric functions into the surface plasmon polariton dispersion relation.[1] This was done for example by Fofang et al.[12] in the simplified case where many of the (background) dielectric constants involved could be taken equal to unity. To generalize this, the dipolar Mie eigenfrequencies of a core−shell particle can be obtained through[81]

$$\varepsilon_2 + 2\varepsilon + \left(\frac{R_1}{R}\right)^3 \frac{2(\varepsilon_1 - \varepsilon_2)(\varepsilon_2 - \varepsilon)}{2\varepsilon_2 + l\varepsilon_1} = 0 \quad (3)$$

where ε_1 is the dielectric function of the core, ε_2 is the corresponding one of the shell, and ε describes the environment, as shown in the schematics of Figure 1. Using the Drude−Lorentz model discussed in the Methods section for ε_1, and a simple Drude model for ε_2 (with plasma frequency equal to 9 eV and background dielectric constant equal to 3.65 to model silver), and disregarding absorptive losses in both materials, as we are interested in the real resonance frequencies, leads to a relation in which ω is raised to the power of 6, and therefore six eigenfrequencies are obtained. Three of them are negative and have no physical meaning; the other three are the two hybrid plasmon−exciton modes, ω_+ and ω_-, shown by open triangles in Figure 1b, and the antisymmetric, cavity-like plasmon mode of the nanoshell,[91] which is at much higher frequencies and does not interact with the exciton.

Apart from the resonance frequency of the two hybrid modes and the width of the Rabi splitting, of particular interest is also the line width of the initial uncoupled modes and that of the hybrid ones. In the description of mechanical harmonic oscillators, the condition for reaching the strong coupling regime is usually defined as $\Omega_R > \omega_{mode}$, where ω_{mode} is the largest frequency between two of the original uncoupled

DOI: 10.1021/acsphotonics.7b00538
ACS Photonics 2018, 5, 133−142

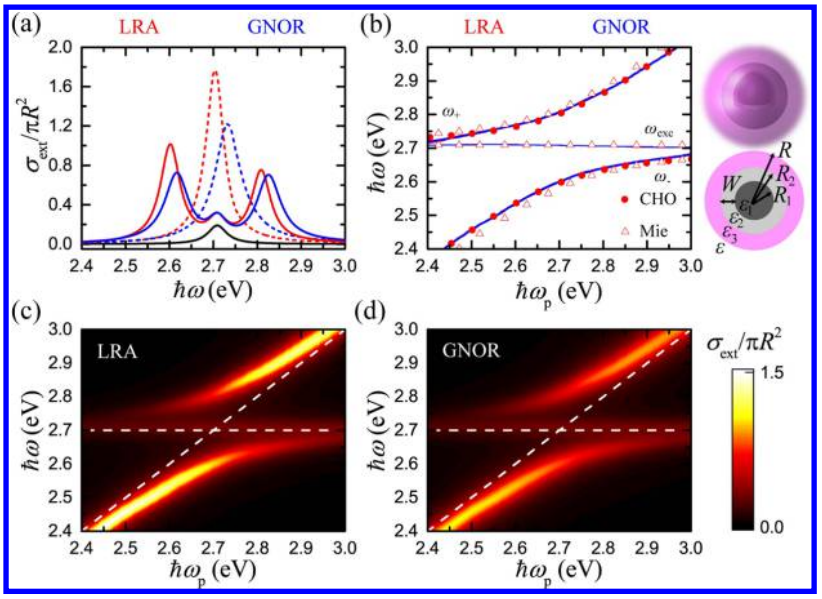

Figure 2. (a) Dipolar particle-like plasmon mode for a nanoshell with R_1 = 5 nm, W = 1.22 nm (see schematics on the right) calculated within LRA (red lines) and GNOR (blue lines) in the absence (dashed lines) or presence (solid lines) of a concentric homogeneous excitonic layer with R = 10 nm and $\hbar\omega_{exc}$ = 2.7 eV. The black solid line depicts the excitonic resonance of the corresponding homogeneous excitonic sphere (R = 10 nm). (b) Energies of the hybrid modes $\omega_\pm$ as a function of $\hbar\omega_p$, within LRA (red lines) and GNOR (blue lines). Red solid dots and open triangles represent the approximate solutions of the CHO model and the Mie expansions, respectively. The thin nearly horizontal line at 2.7 eV is the uncoupled excitonic resonance supported by the outer surface of the particle. Extinction contour plots and the corresponding uncoupled plasmon and exciton energies (white dashed lines) are shown in (c) and (d) for the LRA and GNOR model, respectively. The two contours share a common color scale.

modes. In other contexts, this condition describes the ultrastrong coupling regime. In plasmonics these requirements are usually relaxed, and strong coupling is defined in a more pragmatic way, through[1]

$$\hbar\Omega_R > \sqrt{\frac{(\hbar\gamma_p)^2}{2} + \frac{(\hbar\gamma_{exc})^2}{2}} \tag{4}$$

This is the condition required for the Rabi splitting to be observable in the spectra, and it indeed holds true in the example studied in Figure 1, as can be verified by introducing the line widths of the uncoupled modes discussed above into eq 4. To better illustrate the broadening and damping of the modes predicted by nonlocal theories, in Figure 1c and d we show contour plots of extinction versus energy, obtained with the LRA and GNOR model, respectively. For all shell thicknesses (and therefore the corresponding plasmon energies) studied here, the two hybrid modes are clearly distinguishable, and the relaxed strong-coupling condition of eq 4 holds. We have repeated the same analysis for several nanoparticle sizes and radius−thickness combinations, even reproducing results in the ultrastrong coupling regime,[58] without observing qualitative or quantitative differences from the above discussion.

As a second example, it is natural to explore the inverse topology, where the excitonic layer grows around a metallic nanoshell, a geometry that is easier to achieve experimentally and has been shown to be preferable for obtaining large Rabi splittings and even entering the ultrastrong coupling regime.[58] In Figure 2 we replace the excitonic core of the nanoshell of Figure 1 with a SiO_2 one (described by a dielectric constant ε_1 = 2.13). We assume a constant nanoshell radius R_2 = 5 nm, covered by an external excitonic layer of thickness $R - R_2$ = 5 nm and exciton energy 2.7 eV as previously, and modify the thickness W of the nanoshell, as shown in the schematics of Figure 2. The extinction spectra of the uncoupled components are shown in Figure 2a, with a black line for the spectrum of a homogeneous excitonic sphere of R = 10 nm and red (blue) dashed lines for the LRA (GNOR) spectra of a silver nanoshell with W = 1.22 nm. A thicker shell than in Figure 1a is required to produce the plasmon resonance at 2.7 eV, since a higher-index dielectric is now used as the core material. The corresponding coupled spectra are shown by solid lines and are characterized by a Rabi splitting $\hbar\Omega_R$ = 0.206 eV. In addition to the two hybrid modes, a third peak of much lower intensity is visible at 2.7 eV, which does not shift at all under nonlocal corrections. This is the surface exciton polariton mode excited at the outer surface of the dye layer, which indeed has no reason to be affected by the plasmon modal shifts.[93] It is always excited for this kind of nanoparticle topology, but it is usually masked by the much stronger peaks of the hybrid modes due to the large size of the plasmonic particles. The small nanoshell dimensions explored here ensure that it is clearly discernible in the extinction spectra. Such modes were recently explored as substitutes for plasmons in metals for applications in nanophotonics.[94]

In Figure 2b we present the corresponding dispersion diagram, as a function of the plasmon energy, similarly to Figure 1b. Given our previous analysis in relation to Figure 1b and the spectra presented in Figure 2a, it is not surprising that the dispersion lines for the LRA and GNOR models are again indistinguishable. The CHO model captures excellently the two hybrid modes, as shown by the red solid dots, but it lacks a description of the uncoupled excitonic mode. This weak resonance is excellently reproduced however by the corresponding Mie-based analytic solutions. Since in this case we study a three-layer nanoparticle, one should in principle obtain the corresponding scattering matrix[95,96] and use appropriate asymptotic expressions[97] to obtain the resonances from its poles. A simpler approximation, which we successfully adopt

DOI: 10.1021/acsphotonics.7b00538
ACS Photonics 2018, 5, 133−142

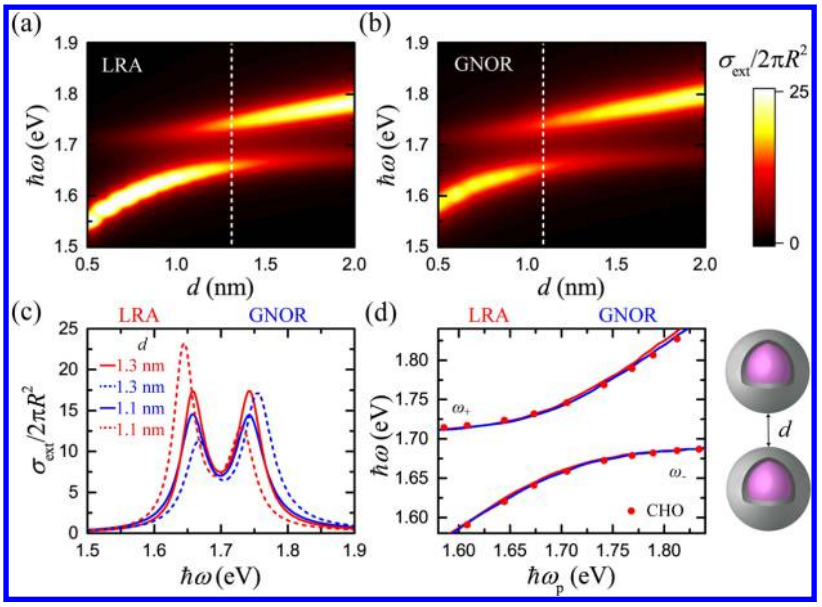

Figure 3. Extinction contour plots as a function of dimer gap width d for the exciton core−silver shell dimers shown in the schematics on the right (R = 20 nm, W = 2 nm), within the LRA (a) and GNOR (b) models. Vertical dashed lines indicate the gap for which the bonding dimer plasmon matches the energy of the exciton ($\hbar\omega_{exc}$ = 1.7 eV). (c) Extinction spectra obtained with the LRA (red lines) and GNOR (blue lines) models, in the presence of an excitonic core, for the gap for which the particular model predicts a plasmon resonance at 1.7 eV (solid lines) and for the d for which the other model is tuned (dashed lines). (d) Dispersion diagram of the two hybrid modes as a function of $\hbar\omega_p$, which is obtained for each model by modifying d in the absence of an excitonic nanoparticle core. Red dots indicate the solutions of the CHO model in the LRA case.

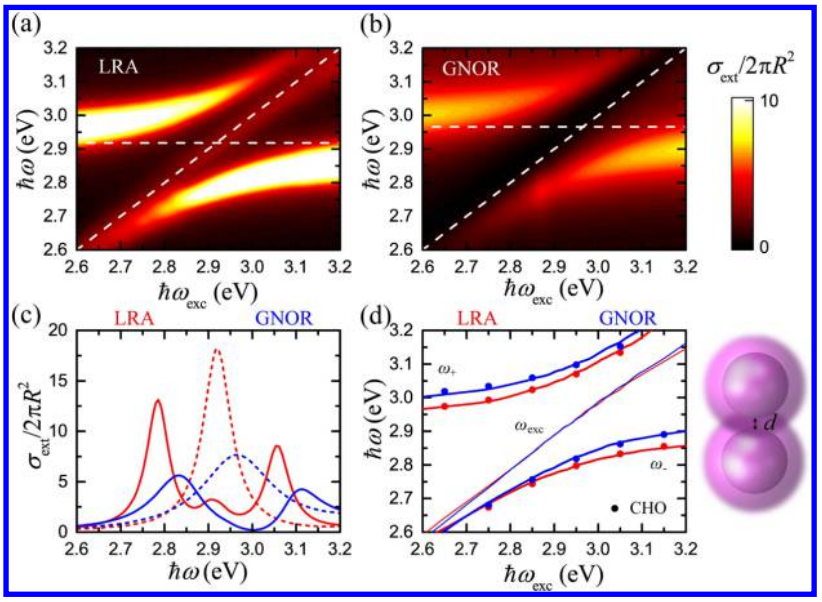

Figure 4. Extinction contour plots as a function of excitonic energy $\hbar\omega_{exc}$ for a silver nanosphere (R = 15 nm) dimer (d = 1 nm) encapsulated in an excitonic matrix, as shown in the schematics on the right, within the LRA (a) and GNOR (b) models. The white dashed lines indicate the uncoupled plasmon and exciton energies. (c) Extinction spectra obtained within LRA (red lines) and GNOR (blue lines), in the absence (dashed lines) or presence (solid lines) of the excitonic matrix. (d) Dispersion diagram of the two hybrid modes as a function of $\hbar\omega_{exc}$. The thin diagonal lines indicate the uncoupled excitonic resonance supported by the outer surface of the excitonic layer. Red and blue solid dots indicate the solutions of the CHO model in the LRA and GNOR case, respectively.

here, is to separate the nanoparticle into two components: a metallic nanoshell embedded in an infinite excitonic environment described by a dielectric function ε_3, for which the hybrid modes $\omega_\pm$ can be obtained from eq 3 (replacing ε with ε_3), and an excitonic sphere of ε_3 in an infinite environment described by ε, for which the resonance condition is[81]

$$\varepsilon_3 + 2\varepsilon = 0 \tag{5}$$

As can be seen by the open triangles in Figure 2b, due to the small sizes involved, this approach works extremely well to accurately describe not only the hybrid modes $\omega_\pm$ but the uncoupled excitonic mode as well. Finally, in Figure 2c and d it is shown through full extinction contours that the additional nonlocal broadening of the modes is not significant in this case either. Considering the initial, uncoupled line widths of the plasmon resonances shown in Figure 2a (0.049 eV for LRA and

DOI: 10.1021/acsphotonics.7b00538
ACS Photonics 2018, 5, 133−142

0.072 eV for GNOR), eq 4 again implies that strong coupling is still achievable under nonlocal corrections.

In the search for a geometry where the footprint of nonlocality might be stronger, we depart from the description of single nanoparticles and study in Figure 3 an exciton core−silver shell dimer. The particles have a total radius R = 20 nm and a metallic shell of thickness D = 2 nm and are separated by a variable gap of width d. Both the thin shell thickness and the narrow dimer gap are expected to enhance nonlocal effects in this case. Instead of tuning the plasmon through the shell thickness, as in Figures 1 and 2, here we change the width of the gap. Plasmon hybridization[91] causes the bonding dimer plasmon modes to red-shift as the gap shrinks,[59] allowing for efficient tuning of the optical response. Extinction contours obtained with the LRA and GNOR models as a function of d are shown in Figure 3a and b, respectively, for an excitonic core with $\hbar\omega_{exc}$ = 1.7 eV. The vertical dashed lines denote the gap for which the bonding dimer plasmon mode in the absence of a dye core is at 1.7 eV and indicate a 0.22 nm difference between the two models. In Figure 3c extinction spectra for each model are presented both for this gap width within the corresponding model (solid lines) and also the gap that tunes the plasmon at 1.7 eV within the other model (dashed lines). Examining the tuned situation for each model, it is evident that no change in the width of the Rabi splitting and no significant broadening can be observed for this geometry either. This is more clear in the dispersion diagram of Figure 3d, where the energy of the hybrid modes is plotted versus the plasmon energy in each model, leading once more to almost identical lines, also in good agreement with the CHO model.

Finally, we turn again to the inverse topology of a dimer enclosed in an excitonic matrix, as shown schematically on the right-hand side of Figure 4. To avoid repetitions and make things more interesting, instead of nanoshells we consider homogeneous silver spheres of radius R = 15 nm separated by a gap of d = 1 nm, covered with an excitonic layer made of two spheres of radius 20 nm, overlapping around the gap, as they are concentric with the corresponding silver particles. In the absence of the excitonic layer the plasmon resonance is found to be at 2.92 eV within LRA and at 2.97 eV within GNOR. Instead of tuning the dimer plasmon through some geometrical parameter, we keep in this case the geometry fixed and modify $\hbar\omega_{exc}$ instead, an approach often adopted in theoretical calculations due to its convenience.[45] Extinction contour maps obtained with LRA and GNOR are shown in Figure 4a and b, respectively, together with the uncoupled excitonic and plasmonic lines (white dashed lines). The corresponding extinction spectra in the presence (solid lines) or absence (dashed lines) of the excitonic layer are shown in Figure 4c. One again observes that the width of the Rabi splitting appears to be nearly unaffected, but the hybrid modes are significantly broadened. Furthermore, the uncoupled excitonic peak, which is strong within LRA, nearly vanishes within GNOR and can only be traced through the corresponding scattering spectra. Nevertheless, this strong damping, originating mainly from the presence of a much larger amount of metallic material (homogeneous spheres instead of shells), is still not enough to bring the system outside the strong coupling regime as defined by eq 4. In addition, careful examination of the dispersion diagrams in Figure 4d shows that the Rabi splitting is in fact narrower by 0.012 eV in the case of GNOR, finally identifying a small impact of nonlocality on the plexcitonic response.

In all the examples explored above, we focused on the dominant, dipolar plasmon modes, which are more relevant from an experimental point of view. While we have identified situations in which our conclusions hold for higher-order modes as well, the coupling of excitons with, for example, quadrupolar single-particle or bonding-dimer modes and how it is affected by nonlocal effects relies on several parameters, and a more systematic study is required. Efficient excitation of higher-order modes in single nanoparticles calls for larger particle sizes, for which nonlocal effects tend to become negligible.[60] On the other hand, for very thin metallic shells, nonlocality can wash out higher-order modes,[80] so that a classically predicted Rabi splitting could disappear completely. Similarly, the efficient excitation of quadrupolar bonding-dimer modes might require entering the truly sub-nanometer regime,[59] where quantum tunneling prevails, restricting nonlocality to a secondary role. Further theoretical work in the future should shed more light on such issues.

To better understand the reason that nonlocal frequency shifts do not usually affect the width of the Rabi splitting, one can recall once more the CHO model of eq 2, according to which the energy difference between the two hybrid modes is

$$\Delta E = \sqrt{{E_R}^2 + (\hbar\omega_p - \hbar\omega_{exc})^2} \tag{6}$$

where $E_R = \hbar\Omega_R$. Nonlocal effects introduce a small correction to the plasmon, $\hbar\omega_p \rightarrow \hbar\omega_p + \delta E$. In the strong-coupling regime, where $\omega_p \simeq \omega_{exc}$, and assuming at a first step that E_R remains constant for simplicity, eq 6 becomes

$$\Delta E \simeq \sqrt{{E_R}^2 + \delta E^2} = E_R\sqrt{1 + \left(\frac{\delta E}{E_R}\right)^2} \tag{7}$$

For Rabi splittings around 0.2 eV and nonlocal blue-shifts on the order of 0.03 eV, typical values in the examples explored here, this introduces a change in δE of about 1%, which is hard to observe. According to the above analysis, one needs to identify systems with much larger nonlocal frequency shifts, accompanied by narrow Rabi splittings, to obtain a strong effect. What is still missing, however, is the influence of nonlocality on the coupling strength and therefore, through $g = 2\hbar\Omega_R$, on the Rabi splitting itself. In a semiclassical approach and as long as the exact positions and orientations of individual emitters in the excitonic layer can be disregarded, the coupling strength is given by[15]

$$g = \mu\sqrt{\frac{N\hbar\omega}{2\varepsilon\varepsilon_0 V}} \tag{8}$$

where N is the number of emitters characterized by a transition dipole moment μ, ω is the transition frequency, ε_0 is the vacuum permittivity, and V is the mode volume. For spherical particles, it has been shown analytically that, for the dipolar mode that is of interest here, the mode volume depends only on the geometrical volume and the environment through $V = (4\pi R^3/3)(1 + 1/2\varepsilon)$.[98] Nevertheless, this result was obtained assuming local response functions for the metal, and nonlocal corrections to V should be evaluated through the general definition[99]

$$V = \frac{\int d^3\mathbf{r}\, u(\mathbf{r})}{\max\{u(\mathbf{r})\}} \tag{9}$$

DOI: 10.1021/acsphotonics.7b00538
ACS Photonics 2018, 5, 133−142

where $u(\mathbf{r})$ is the electromagnetic energy density at position $\mathbf{r}$. Introducing nonlocal corrections into eq 9 has been discussed in detail by Toscano et al.[100] Our calculations have shown that within the GNOR model V typically increases by no more than 20%, which translates into a ∼10% decrease in the coupling strength. Since this modification enters eq 6 through a $E_R \rightarrow E_R - \delta E_R$ correction, the nonlocal changes in coupling strength and plasmon energy tend, to first order, to cancel each other out. This tendency is further strengthened once absorptive losses are taken into account, which, according to eq 1, introduce an extra damping correction $\delta\gamma$, working toward the same direction as δE in eq 7, to further counterbalance the (relatively stronger) effect of increasing the mode volume. In view of the above discussion, interpreting the results of Figures 1−4 and understanding why nonlocal effects do not usually play an important role in the exciton−plasmon coupling can be achieved in a simple and intuitive manner.

CONCLUSIONS

In summary, we explored the influence of nonlocal effects in the description of the metal on the coupling of plasmonic nanoparticles with dye layers characterized by an excitonic transition. Through detailed simulations, in conjunction with analytical modeling, we showed that, contrary to expectations based mainly on results for single emitters in plasmonic environments, neither nonlocal frequency shifts due to screening nor surface-enhanced Landau damping produces strong deviations from a description within classical electrodynamics. Apart from extreme situations of dramatic nonlocal blue-shifts in situations of already narrow Rabi splittings, nonlocality affects plasmon−exciton coupling only incrementally, as long as the excitonic material is sufficiently described as a homogeneous layer. For simplicity, we have used here the GNOR model, leaving quantum corrections based on the Feibelman parameters for the centroid of charge or on surface-dipole moments for future investigation.[74,77] By analyzing how nonlocal corrections in plasmonics enter into the common coupled-oscillator model, we provided a simple, intuitive interpretation of our findings. Novel plexcitonic architectures involving reduced, few-nanometer length scales can be analyzed without the necessity to resort to elaborate models going beyond classical electrodynamics, thus providing additional flexibility in the design and optimization of systems with strong light−matter interactions.

METHODS

Homogeneous silver nanoparticles and thin silver shells are described by the experimental dielectric function ε_{exp} of Johnson and Christy.[101] When nonlocal corrections are introduced in the metal, the Drude part is subtracted from ε_{exp} to produce the background contribution to the metal dielectric function, ε_∞, according to

$$\varepsilon_{Drude} = \varepsilon_\infty - \frac{{\omega_p}^2}{\omega(\omega + i\gamma_p)}, \quad \varepsilon_\infty = \varepsilon_{exp} + \frac{{\omega_p}^2}{\omega(\omega + i\gamma_p)} \tag{10}$$

where for silver we use $\hbar\omega_p = 8.99$ eV, $\hbar\gamma_p = 0.025$ eV.[65]

In the case of single nanoparticles, we include nonlocal corrections in the scattering matrix of the Mie solution as described by Tserkezis et al.[102] For a homogeneous metallic sphere of radius R described by a dielectric function ε_1 in a homogeneous medium of ε_2 the electric-type nonlocal Mie coefficients of multipole order l, t_l^{TM}, are given by

$$t_l^{TM} = \frac{-\varepsilon_1 j_l(x_1)[x_2 j_l(x_2)]' + \varepsilon_2 j_l(x_2)\{[x_1 j_l(x_1)]' + \Delta_l\}}{\varepsilon_1 j_l(x_1)[x_2 h_l^+(x_2)]' - \varepsilon_2 h_l^+(x_2)\{[x_1 j_l(x_1)]' + \Delta_l\}} \tag{11}$$

where $j_l(x)$ and $h_l^+(x)$ are the spherical Bessel and first-type Hankel functions, respectively, while $x_i = q_i R$ with q_i being the (transverse) wavenumber in medium i and $'$ denotes derivation with respect to the argument. The nonlocal correction Δ_l to the Mie coefficients is given as

$$\Delta_l = l(l+1) j_l(x_1) \frac{\varepsilon_1 - \varepsilon_\infty}{\varepsilon_\infty} \frac{j_l(x_L)}{x_L j_l'(x_L)} \tag{12}$$

where $x_L = q_L R$ and q_L is the longitudinal wavenumber in the sphere, associated with the longitudinal dielectric function ε_L, which is frequency- and wave vector-dependent.[62,103] The dispersion of longitudinal waves is given by $\varepsilon_L(\omega, \mathbf{q}) = 0$. In the limiting case where $\Delta_l = 0$ we retrieve the local result of standard Mie theory. The corresponding analytical solution is lengthy and can be found in the Supporting Information of the paper by Tserkezis et al.[80]

In the case of dimers, we use a commercial finite-element solver (Comsol Multiphysics 5.0),[104] appropriately adapted to include the description of nonlocal effects,[105] to solve the system of coupled equations[85]

$$\nabla \times \nabla \times \mathbf{E}(\mathbf{r}, \omega) = \left(\frac{\omega}{c}\right)^2 \varepsilon_\infty \mathbf{E}(\mathbf{r}, \omega) + i\omega\mu_0 \mathbf{J}(\mathbf{r}, \omega)$$

$$\left[\frac{\beta^2}{\omega(\omega + i\gamma)} + \frac{D}{i\omega}\right] \nabla[\nabla \cdot \mathbf{J}(\mathbf{r}, \omega)] + \mathbf{J}(\mathbf{r}, \omega) = \sigma \mathbf{E}(\mathbf{r}, \omega) \tag{13}$$

where $\mathbf{E}$ and $\mathbf{J}$ are the electric field and the induced current density, respectively; $\sigma = i\varepsilon_0 {\omega_p}^2/(\omega + i\gamma_p)$ is the Drude conductivity, and μ_0 is the vacuum permeability, related to the velocity of light in a vacuum through $c = 1/\sqrt{\varepsilon_0\mu_0}$.

In both approaches, the hydrodynamic parameter β is taken equal to $\sqrt{3/5}\, v_F$, where $v_F = 1.39 \times 10^6$ m s^{-1} is the Fermi velocity of silver,[65] while for the diffusion constant D we use $D = 2.684 \times 10^4$ m^2 s^{-1}.[102] Values of this order of magnitude reproduce well the experimentally observed size-dependent broadening in small metallic nanoparticles.[106] As the additional boundary condition we adopt the usual condition of zero normal component of the induced current density at the metal boundary,[65] which implies a hard-wall description of the metal, an approach which might prove inefficient in the case of good jellium metals,[107,108] but is reasonable for a noble metal with high work function such as silver. When describing the interface between silver and the excitonic layer, we assume that carriers from one medium are not allowed to enter the other, an assumption justified by the fact that the excitonic layer consists of an assembly of dye molecules and is only effectively described as a homogeneous layer.

For the excitonic material we use a Drude−Lorentz model according to

$$\varepsilon = 1 - \frac{f{\omega_{exc}}^2}{\omega^2 - {\omega_{exc}}^2 + i\omega\gamma_{exc}} \tag{14}$$

DOI: 10.1021/acsphotonics.7b00538
ACS Photonics 2018, 5, 133−142

where f is the reduced oscillator strength. Throughout the paper ω_{exc} is allowed to vary as stated in each case, $f = 0.02$, and $\hbar\gamma_{exc} = 0.052$ eV.[12]

AUTHOR INFORMATION

Corresponding Authors

*E-mail (C. Tserkezis): ctse@fotonik.dtu.dk.
*E-mail (M. Wubs): mwubs@fotonik.dtu.dk.
*E-mail (N. A. Mortensen): asger@mailaps.org.

ORCID

Christos Tserkezis: 0000-0002-2075-9036
N. Asger Mortensen: 0000-0001-7936-6264

Notes

The authors declare no competing financial interest.

ACKNOWLEDGMENTS

C.T. was supported by funding from the People Programme (Marie Curie Actions) of the European Union's Seventh Framework Programme (FP7/2007-2013) under REA grant agreement number 609405 (COFUNDPostdocDTU). We gratefully acknowledge support from VILLUM Fonden via the VKR Centre of Excellence NATEC-II and from the Danish Council for Independent Research (FNU 1323-00087). The Center for Nanostructured Graphene (CNG) was financed by the Danish National Research Council (DNRF103). N.A.M. is a VILLUM Investigator supported by VILLUM Fonden.

REFERENCES

(1) Törmä, P.; Barnes, W. L. Strong coupling between surface plasmon polaritons and emitters: a review. *Rep. Prog. Phys.* **2015**, *78*, 013901.

(2) Moerland, R. J.; Hakala, T. K.; Martikainen, J.-P.; Rekola, H. T.; Väkeväinen, A. I.; Törmä, P. In *Quantum Plasmonics*; Bozhevolnyi, S. I., Martín-Moreno, L., García-Vidal, F. J., Eds.; Springer Series in Solid-State Sciences; Springer International Publishing: Cham, 2017; Vol. *185*; Chapter Strong coupling between organic molecules and plasmonic nanostructure, pp 121−150.

(3) Pockrand, I.; Brillante, A.; Möbius, D. Exciton-surface plasmon coupling: an experimental investigation. *J. Chem. Phys.* **1982**, *77*, 6289−6295.

(4) Bellessa, J.; Bonnand, C.; Plenet, J. C.; Mugnier, J. Strong coupling between surface plasmons and excitons in an organic semiconductor. *Phys. Rev. Lett.* **2004**, *93*, 036404.

(5) Dintinger, J.; Klein, S.; Bustos, F.; Barnes, W. L.; Ebbesen, T. W. Strong coupling between surface plasmon-polaritons and organic molecules in subwavelength hole arrays. *Phys. Rev. B: Condens. Matter Mater. Phys.* **2005**, *71*, 035424.

(6) Hakala, T. K.; Toppari, J. J.; Kuzyk, A.; Pettersson, M.; Tikkanen, H.; Kunttu, H.; Törmä, P. Vacuum Rabi splitting and strong-coupling dynamics for surface-plasmon polaritons and Rhodamine 6G molecules. *Phys. Rev. Lett.* **2009**, *103*, 053602.

(7) Gómez, D. E.; Vernon, K. C.; Mulvaney, P.; Davis, T. J. Surface plasmon mediated strong exciton-photon coupling in semiconductor nanocrystals. *Nano Lett.* **2010**, *10*, 274−278.

(8) González-Tudela, A.; Huidobro, P. A.; Martín-Moreno, L.; Tejedor, C.; García-Vidal, F. J. Theory of strong coupling between quantum emitters and propagating surface plasmons. *Phys. Rev. Lett.* **2013**, *110*, 126801.

(9) Tumkur, T. U.; Zhu, G.; Noginov, M. A. Strong coupling of surface plasmon polaritons and ensembles of dye molecules. *Opt. Express* **2016**, *24*, 3921−3928.

(10) Wiederrecht, G. P.; Wurtz, G. A.; Hranisavljevic, J. Coherent coupling of molecular excitons to electronic polarizations of noble metal nanoparticles. *Nano Lett.* **2004**, *4*, 2121−2125.

(11) Sugawara, Y.; Kelf, T. A.; Baumberg, J. J.; Abdelsalam, M. E.; Bartlett, P. N. Strong coupling between localized plasmons and organic excitons in metal nanovoids. *Phys. Rev. Lett.* **2006**, *97*, 266808.

(12) Fofang, N. T.; Park, T.-H.; Neumann, O.; Mirin, N. A.; Nordlander, P.; Halas, N. J. Plexcitonic nanoparticles: plasmon-exciton coupling in nanoshell-J-aggregate complexes. *Nano Lett.* **2008**, *8*, 3481−3487.

(13) Trügler, A.; Hohenester, U. Strong coupling between a metallic nanoparticle and a single molecule. *Phys. Rev. B: Condens. Matter Mater. Phys.* **2008**, *77*, 115403.

(14) Zengin, G.; Johansson, G.; Johansson, P.; Antosiewicz, T. J.; Käll, M.; Shegai, T. Approaching the strong coupling limit in single plasmonic nanorods interacting with J-aggregates. *Sci. Rep.* **2013**, *3*, 3074.

(15) Zengin, G.; Wersäll, M.; Nilsson, S.; Antosiewicz, T. J.; Käll, M.; Shegai, T. Realizing strong light-matter interactions between single-nanoparticle plasmons and molecular excitons at ambient conditions. *Phys. Rev. Lett.* **2015**, *114*, 157401.

(16) Melnikau, D.; Esteban, R.; Savateeva, D.; Sánchez-Iglesias, A.; Grzelczak, M.; Schmidt, M. K.; Liz-Marzán, L. M.; Aizpurua, J.; Rakovich, Y. P. Rabi splitting in photoluminescence spectra of hybrid systems of gold nanorods and J-aggregates. *J. Phys. Chem. Lett.* **2016**, *7*, 354−362.

(17) Lidzey, D. G.; Bradley, D. D. C.; Skolnick, M. S.; Virgili, T.; Walker, S.; Whittaker, D. M. Strong exciton-photon coupling in an organic semiconductor microcavity. *Nature* **1998**, *395*, 53−55.

(18) Chang, D. E.; Sørensen, A. S.; Hemmer, P. R.; Lukin, M. D. Strong coupling of single emitters to surface plasmons. *Phys. Rev. B: Condens. Matter Mater. Phys.* **2007**, *76*, 035420.

(19) Delga, A.; Feist, J.; Bravo-Abad, J.; García-Vidal, F. J. Quantum emitters near a metal nanoparticle: strong coupling and quenching. *Phys. Rev. Lett.* **2014**, *112*, 253601.

(20) George, J.; Wang, S.; Chervy, T.; Canaguier-Durand, A.; Schaeffer, G.; Lehn, J.-M.; Hutchison, J. A.; Genet, C.; Ebbesen, T. W. Ultra-strong coupling of molecular materials: spectroscopy and dynamics. *Faraday Discuss.* **2015**, *178*, 281−294.

(21) Tanyi, E. K.; Thuman, H.; Brown, N.; Koutsares, S.; Podolskiy, V. A.; Noginov, M. A. Control of the Stokes shift with strong coupling. *Adv. Opt. Mater.* **2017**, *5*, 1600941.

(22) Bozhevolnyi, S. I., Martín-Moreno, L., García-Vidal, F. J., Eds. *Quantum Plasmonics*; Springer Series in Solid-State Sciences; Springer International Publishing: Cham, 2017; Vol. *185*.

(23) Bozhevolnyi, S. I.; Mortensen, N. A. Plasmonics for emerging quantum technologies. *Nanophotonics* **2017**, *6*, 1185−1188.

(24) Hobson, P. A.; Wedge, S.; Wasey, J. A. E.; Sage, I.; Barnes, W. L. Surface plasmon mediated emission from organic light-emitting diodes. *Adv. Mater.* **2002**, *14*, 1393−1396.

(25) Dintinger, J.; Robel, I.; Kamat, P. V.; Genet, C.; Ebbesen, T. W. Terahertz all-optical molecule-plasmon modulation. *Adv. Mater.* **2006**, *18*, 1645−1648.

(26) Chang, D. E.; Sørensen, A. S.; Demler, E. A.; Lukin, M. D. A single-photon transistor using nanoscale surface plasmons. *Nat. Phys.* **2007**, *3*, 807−812.

(27) Auffèves, A.; Gérard, J.-M.; Poizat, J.-P. Pure emitter dephasing: a resource for advanced solid-state single-photon sources. *Phys. Rev. A: At., Mol., Opt. Phys.* **2009**, *79*, 053838.

(28) Schwartz, T.; Hutchison, J. A.; Genet, C.; Ebbesen, T. W. Reversible switching of ultrastrong light-molecule coupling. *Phys. Rev. Lett.* **2011**, *106*, 196405.

(29) Thompson, R. J.; Rempe, G.; Kimble, H. J. Observation of normal-mode splitting for an atom in an optical cavity. *Phys. Rev. Lett.* **1992**, *68*, 1132−1135.

(30) Yoshie, T.; Scherer, A.; Hendrickson, J.; Khitrova, G.; Gibbs, H. M.; Rupper, G.; Ell, C.; Shchekin, O. B.; Deppe, D. G. Vacuum Rabi splitting with a single quantum dot in a photonic crystal nanocavity. *Nature* **2004**, *432*, 200−203.

(31) Aoki, T.; Dayan, B.; Wilcut, E.; Bowen, W. P.; Parkins, A. S.; Kippenberg, T. J.; Vahala, K. J.; Kimble, H. J. Observation of strong

DOI: 10.1021/acsphotonics.7b00538
ACS Photonics 2018, 5, 133−142

coupling between one atom and a monolithic microresonator. *Nature* **2006**, *443*, 671−674.
(32) Faraon, A.; Fushman, I.; Englund, D.; Stoltz, N.; Petroff, P.; Vučković, J. Coherent generation of non-classical light on a chip via photon-induced tunnelling and blockade. *Nat. Phys.* **2008**, *4*, 859−863.
(33) Lidzey, D. G.; Bradley, D. D. C.; Armitage, A.; Walker, S.; Skolnick, M. S. Photon-mediated hybridization of Frenkel excitons in organic semiconductor microcavities. *Science* **2000**, *288*, 1620−1623.
(34) Schuller, J. A.; Barnard, E. S.; Cai, W.; Jun, Y. C.; White, J. S.; Brongersma, M. L. Plasmonics for extreme light concentration and manipulation. *Nat. Mater.* **2010**, *9*, 193−204.
(35) Santhosh, K.; Bitton, O.; Chuntonov, L.; Haran, G. Vacuum Rabi splitting in a plasmonic cavity at the single quantum emitter limit. *Nat. Commun.* **2016**, *7*, 11823.
(36) Chikkaraddy, R.; de Nijs, B.; Benz, F.; Barrow, S. J.; Scherman, O. A.; Rosta, E.; Demetriadou, A.; Fox, P.; Hess, O.; Baumberg, J. J. Single-molecule strong coupling at room temperature in plasmonic nanocavities. *Nature* **2016**, *535*, 127−130.
(37) Vasa, P.; Wang, W.; Pomraenke, R.; Lammers, M.; Maiuri, M.; Manzoni, C.; Cerullo, G.; Lienau, C. Real-time observation of ultrafast Rabi oscillations between excitons and plasmons in metal nanostructures with J-aggregates. *Nat. Photonics* **2013**, *7*, 128−132.
(38) Vasa, P.; Wang, W.; Pomraenke, R.; Maiuri, M.; Manzoni, C.; Cerullo, G.; Lienau, C. Optical Stark effects in J-aggregate-metal hybrid nanostructures exhibiting a strong exciton-surface-plasmon-polariton interaction. *Phys. Rev. Lett.* **2015**, *114*, 036802.
(39) Wang, H.; Wang, H.-Y.; Bozzola, A.; Toma, A.; Panaro, S.; Raja, W.; Alabastri, A.; Wang, L.; Chen, Q.-D.; Xu, H.-L.; De Angelis, F.; Sun, H.-B.; Zaccaria, R. P. Dynamics of strong coupling between J-aggregates and surface plasmon polaritons in subwavelength hole arrays. *Adv. Funct. Mater.* **2016**, *26*, 6198−6205.
(40) Waks, E.; Sridharan, D. Cavity QED treatment of interactions between a metal nanoparticle and a dipole emitter. *Phys. Rev. A: At., Mol., Opt. Phys.* **2010**, *82*, 043945.
(41) Liu, R.; Zhou, Z.-K.; Yu, Y.-C.; Zhang, T.; Wang, H.; Liu, G.; Wei, Y.; Chen, H.; Wang, X.-H. Strong light-matter interactions in single open plasmonic nanocavities at the quantum optics limit. *Phys. Rev. Lett.* **2017**, *118*, 237401.
(42) Savasta, S.; Saija, R.; Ridolfo, A.; Di Stefano, O.; Denti, P.; Borghese, F. Nanopolaritons: vacuum Rabi splitting with a single quantum dot in the center of a dimer nanoantenna. *ACS Nano* **2010**, *4*, 6369−6376.
(43) Manjavacas, A.; García de Abajo, F. J.; Nordlander, P. Quantum plexcitonics: strongly interacting plasmons and excitons. *Nano Lett.* **2011**, *11*, 2318−2323.
(44) Schlather, A. E.; Large, N.; Urban, A. S.; Nordlander, P.; Halas, N. J. Near-field mediated plexcitonic coupling and giant Rabi splitting in individual metallic dimers. *Nano Lett.* **2013**, *13*, 3281−3286.
(45) Pérez-González, O.; Zabala, N.; Aizpurua, J. Optical properties and sensing in plexcitonic nanocavities: from simple molecular linkers to molecular aggregate layers. *Nanotechnology* **2014**, *25*, 035201.
(46) Roller, E.-M.; Argyropoulos, C.; Högele, A.; Liedl, T.; Pilo-Pais, M. Plasmon-exciton coupling using DNA templates. *Nano Lett.* **2016**, *16*, 5962−5966.
(47) Li, R.-Q.; Hernángomez-Pérez, D.; García-Vidal, F. J.; Fernández-Domínguez, A. I. Transformation optics approach to plasmon-exciton strong coupling in nanocavities. *Phys. Rev. Lett.* **2016**, *117*, 107401.
(48) Chen, X.; Chen, Y.-H.; Qin, J.; Zhao, D.; Ding, B.; Blaikie, R. J.; Qiu, M. Mode modification of plasmonic gap resonances induced by strong coupling with molecular excitons. *Nano Lett.* **2017**, *17*, 3246−3251.
(49) Wurtz, G. A.; Evans, P. R.; Hendren, W.; Atkinson, R.; Dickson, W.; Pollard, R. J.; Zayats, A. V. Molecular plasmonics with tunable exciton-plasmon coupling strength in J-aggregate hybridized Au nanorod assemblies. *Nano Lett.* **2007**, *7*, 1297−1303.
(50) Eizner, E.; Avayu, O.; Ditcovski, R.; Ellenbogen, T. Aluminum nanoantenna complexes for strong coupling between excitons and localized surface plasmons. *Nano Lett.* **2015**, *15*, 6215−6221.
(51) Tsargorodska, A.; Cartron, M. L.; Vasilev, C.; Kodali, G.; Mass, O. A.; Baumberg, J. J.; Dutton, P. L.; Hunter, C. N.; Törmä, P.; Leggett, G. J. Strong coupling of localized surface plasmons to excitons in light-harvesting complexes. *Nano Lett.* **2016**, *16*, 6850−6856.
(52) Todisco, F.; Esposito, M.; Panaro, S.; De Giorgi, M.; Dominici, L.; Ballarini, D.; Fernández-Domínguez, A. I.; Tasco, V.; Cuscunà, M.; Passaseo, A.; Ciracì, C.; Gigli, G.; Sanvitto, D. Toward cavity quantum electrodynamics with hybrid photon gap-plasmon states. *ACS Nano* **2016**, *10*, 11360−11368.
(53) Li, J.; Ueno, K.; Uehara, H.; Guo, J.; Oshikiri, T.; Misawa, H. Dual strong couplings between TPPS J-aggregates and aluminum plasmonic states. *J. Phys. Chem. Lett.* **2016**, *7*, 2786−2791.
(54) Esteban, R.; Aizpurua, J.; Bryant, G. W. Strong coupling of single emitters interacting with phononic infrared antennae. *New J. Phys.* **2014**, *16*, 013052.
(55) Ren, J.; Gu, Y.; Zhao, D.; Zhang, F.; Zhang, T.; Gong, Q. Evanescent-vacuum-enhanced photon-exciton coupling and fluorescence collection. *Phys. Rev. Lett.* **2017**, *118*, 073604.
(56) Geiser, M.; Castellano, F.; Scalari, G.; Beck, M.; Nevou, L.; Faist, J. Ultrastrong coupling regime and plasmon polaritons in parabolic semiconductor quantum wells. *Phys. Rev. Lett.* **2012**, *108*, 106402.
(57) Balci, S. Ultrastrong plasmon-exciton coupling in metal nanoprisms with J-aggregates. *Opt. Lett.* **2013**, *38*, 4498−4501.
(58) Cacciola, A.; Di Stefano, O.; Stassi, R.; Saija, R.; Savasta, S. Ultrastrong coupling of plasmons and excitons in a nanoshell. *ACS Nano* **2014**, *8*, 11483−11492.
(59) Romero, I.; Aizpurua, J.; Bryant, G. W.; García de Abajo, F. J. Plasmons in nearly touching metallic nanoparticles: singular response in the limit of touching dimers. *Opt. Express* **2006**, *14*, 9988−9999.
(60) Raza, S.; Kadkhodazadeh, S.; Christensen, T.; di Vece, M.; Wubs, M.; Mortensen, N. A.; Stenger, N. Multipole plasmons and their disappearance in few-nanometre silver nanoparticles. *Nat. Commun.* **2015**, *6*, 8788.
(61) Zhu, W.; Esteban, R.; Borisov, A. G.; Baumberg, J. J.; Nordlander, P.; Lezec, H. J.; Aizpurua, J.; Crozier, K. B. Quantum mechanical effects in plasmonic structures with subnanometre gaps. *Nat. Commun.* **2016**, *7*, 11495.
(62) García de Abajo, F. J. Nonlocal effects in the plasmons of strongly interacting nanoparticles, dimers, and waveguides. *J. Phys. Chem. C* **2008**, *112*, 17983−17987.
(63) McMahon, J. M.; Gray, S. K.; Schatz, G. C. Nonlocal optical response of metal nanostructures with arbitrary shape. *Phys. Rev. Lett.* **2009**, *103*, 097403.
(64) Raza, S.; Toscano, G.; Jauho, A.-P.; Wubs, M.; Mortensen, N. A. Unusual resonances in nanoplasmonic structures due to nonlocal response. *Phys. Rev. B: Condens. Matter Mater. Phys.* **2011**, *84*, 121412.
(65) Raza, S.; Bozhevolnyi, S. I.; Wubs, M.; Mortensen, N. A. Nonlocal optical response in metallic nanostructures. *J. Phys.: Condens. Matter* **2015**, *27*, 183204.
(66) Li, X.; Xiao, D.; Zhang, Z. Landau damping of quantum plasmons in metal nanostructures. *New J. Phys.* **2013**, *15*, 023011.
(67) Khurgin, J. B. Ultimate limit of field confinement by surface plasmon polaritons. *Faraday Discuss.* **2015**, *178*, 109−122.
(68) Shahbazyan, T. V. Landau damping of surface plasmons in metal nanostructures. *Phys. Rev. B: Condens. Matter Mater. Phys.* **2016**, *94*, 235431.
(69) Weick, G.; Ingold, G.-L.; Jalabert, R. A.; Weinmann, D. Surface plasmon in metallic nanoparticles: renormalization effects due to electron-hole excitations. *Phys. Rev. B: Condens. Matter Mater. Phys.* **2006**, *74*, 165421.
(70) Scholl, J. A.; Koh, A. L.; Dionne, J. A. Quantum plasmon resonances of individual metallic nanoparticles. *Nature* **2012**, *483*, 421−427.
(71) Monreal, R. C.; Antosiewicz, T. J.; Apell, S. P. Competition between surface screening and size quantization for surface plasmons in nanoparticles. *New J. Phys.* **2015**, *15*, 083044.
(72) Toscano, G.; Straubel, J.; Kwiatkowski, A.; Rockstuhl, C.; Evers, F.; Xu, H.; Mortensen, N. A.; Wubs, M. Resonance shifts and spill-out

DOI: 10.1021/acsphotonics.7b00538
ACS Photonics 2018, 5, 133−142

effects in self-consistent hydrodynamic nanoplasmonics. *Nat. Commun.* **2015**, *6*, 7132.
(73) Ciracì, C.; della Sala, F. Quantum hydrodynamic theory for plasmonics: Impact of the electron density tail. *Phys. Rev. B: Condens. Matter Mater. Phys.* **2016**, *93*, 205405.
(74) Christensen, T.; Yan, W.; Jauho, A.-P.; Soljačić, M.; Mortensen, N. A. Quantum corrections in nanoplasmonics: shape, scale, and material. *Phys. Rev. Lett.* **2017**, *118*, 157402.
(75) Savage, K. J.; Hawkeye, M. M.; Esteban, R.; Borisov, A. G.; Aizpurua, J.; Baumberg, J. J. Revealing the quantum regime in tunnelling plasmonics. *Nature* **2012**, *491*, 574−577.
(76) Scholl, J. A.; García-Etxarri, A.; Koh, A. L.; Dionne, J. A. Observation of quantum tunneling between two plasmonic nanoparticles. *Nano Lett.* **2013**, *13*, 564−569.
(77) Yan, W.; Wubs, M.; Mortensen, N. A. Projected dipole model for quantum plasmonics. *Phys. Rev. Lett.* **2015**, *115*, 137403.
(78) Filter, R.; Bösel, C.; Toscano, G.; Lederer, F.; Rockstuhl, C. Nonlocal effects: relevance for the spontaneous emission rates of quantum emitters coupled to plasmonic structures. *Opt. Lett.* **2014**, *39*, 6118−6121.
(79) Raza, S.; Wubs, M.; Bozhevolnyi, S. I.; Mortensen, N. A. Nonlocal study of ultimate plasmon hybridization. *Opt. Lett.* **2015**, *40*, 839−842.
(80) Tserkezis, C.; Stefanou, N.; Wubs, M.; Mortensen, N. A. Molecular fluorescence enhancement in plasmonic environments: exploring the role of nonlocal effects. *Nanoscale* **2016**, *8*, 17532−17541.
(81) Tserkezis, C.; Mortensen, N. A.; Wubs, M. How nonlocal damping reduces plasmon-enhanced fluorescence in ultranarrow gaps. *Phys. Rev. B: Condens. Matter Mater. Phys.* **2017**, *96*, 085413.
(82) Marinica, D. C.; Lourenço-Martins, H.; Aizpurua, J.; Borisov, A. G. Plexciton quenching by resonant electron transfer from quantum emitter to metallic nanoantenna. *Nano Lett.* **2013**, *13*, 5972−5978.
(83) Ciracì, C.; Hill, R. T.; Mock, J. J.; Urzhumov, Y.; Fernández-Domínguez, A. I.; Maier, S. A.; Pendry, J. B.; Chilkoti, A.; Smith, D. R. Probing the ultimate limits of plasmonic enhancement. *Science* **2012**, *337*, 1072−1074.
(84) Shen, H.; Chen, L.; Ferrari, L.; Lin, M.-H.; Mortensen, N. A.; Gwo, S.; Liu, Z. Optical observation of plasmonic nonlocal effects in a 2D superlattice of ultrasmall gold nanoparticles. *Nano Lett.* **2017**, *17*, 2234−2239.
(85) Mortensen, N. A.; Raza, S.; Wubs, M.; Søndergaard, T.; Bozhevolnyi, S. I. A generalized non-local optical response theory for plasmonic nanostructures. *Nat. Commun.* **2014**, *5*, 3809.
(86) Wubs, M.; Mortensen, N. A. In *Quantum Plasmonics*; Bozhevolnyi, S. I., Martín-Moreno, L., García-Vidal, F. J., Eds.; Springer Series in Solid-State Sciences; Springer International Publishing: Cham, 2017; Vol. *185*; Chapter Nonlocal response in plasmonic nanostructures, pp 279−302.
(87) Zhang, X.; Guo, L.; Luo, J.; Zhao, X.; Wang, T.; Li, Y.; Fu, Y. Metallic nanoshells with sub-10 nm thickness and their performance as surface-enhanced spectroscopy substrate. *ACS Appl. Mater. Interfaces* **2016**, *8*, 9889−9896.
(88) Tserkezis, C.; Gantzounis, G.; Stefanou, N. Collective plasmonic modes in ordered assemblies of metallic nanoshells. Matter. *J. Phys.: Condens. Matter* **2008**, *20*, 075232.
(89) Raza, S.; Toscano, G.; Jauho, A.-P.; Mortensen, N. A.; Wubs, M. Refractive-index sensing with ultrathin plasmonic nanotubes. *Plasmonics* **2013**, *8*, 193−199.
(90) Oldenburg, S. J.; Averitt, R. D.; Westcott, S. L.; Halas, N. J. Nanoengineering of optical resonances. *Chem. Phys. Lett.* **1998**, *288*, 243−247.
(91) Prodan, E.; Radloff, C.; Halas, N. J.; Nordlander, P. A hybridization model for the plasmon response of complex nanostructures. *Science* **2003**, *302*, 419−422.
(92) Rudin, S.; Reinecke, T. L. Oscillator model for vacuum Rabi splitting in microcavities. *Phys. Rev. B: Condens. Matter Mater. Phys.* **1999**, *59*, 10227−10233.
(93) Philpott, M. R.; Brillante, A.; Pockrand, I. R.; Swalen, J. D. A new optical phenomenon: exciton surface polaritons at room temperature. *Mol. Cryst. Liq. Cryst.* **1979**, *50*, 139−162.
(94) Gentile, M. J.; Barnes, W. L. Hybridised exciton-polariton resonances in core-shell nanoparticles. *J. Opt.* **2017**, *19*, 035003.
(95) Bohren, C. F.; Huffman, D. R. *Absorption and Scattering of Light by Small Particles*; Wiley: New York, 1983.
(96) Stefanou, N.; Tserkezis, C.; Gantzounis, G. Plasmonic excitations in ordered assemblies of metallic nanoshells. *Proc. SPIE* **2008**, *6989*, 698910.
(97) Arfken, G. B.; Weber, H. J. *Mathematical Methods for Physicist*, 5th ed.; Academic Press: San Diego, 2000.
(98) Khurgin, J. B.; Sun, G. Enhancement of optical properties of nanoscaled objects by metal nanoparticles. *J. Opt. Soc. Am. B* **2009**, *26*, B83−B95.
(99) Maier, S. A. Plasmonic field enhancement and SERS in the effective mode volume picture. *Opt. Express* **2006**, *14*, 1957−1964.
(100) Toscano, G.; Raza, S.; Yan, W.; Jeppesen, C.; Xiao, S.; Wubs, M.; Jauho, A.-P.; Bozhevolnyi, S. I.; Mortensen, N. A. Nonlocal response in plasmonic waveguiding with extreme light confinement. *Nanophotonics* **2013**, *2*, 161−166.
(101) Johnson, P. B.; Christy, R. W. Optical constants of the noble metals. *Phys. Rev. B* **1972**, *6*, 4370−4379.
(102) Tserkezis, C.; Maack, J. R.; Liu, Z.; Wubs, M.; Mortensen, N. A. Robustness of the far-field response of nonlocal plasmonic ensembles. *Sci. Rep.* **2016**, *6*, 28441.
(103) Ruppin, R. Optical properties of a plasma sphere. *Phys. Rev. Lett.* **1973**, *31*, 1434−1347.
(104) Comsol Multiphysics, www.comsol.com.
(105) Nanoplasmonics Lab, www.nanopl.org.
(106) Kreibig, U.; Genzel, L. Optical absorption of small metallic particles. *Surf. Sci.* **1985**, *156*, 678−700.
(107) Teperik, T. V.; Nordlander, P.; Aizpurua, J.; Borisov, A. G. Robust subnanometric plasmon ruler by rescaling of the nonlocal optical response. *Phys. Rev. Lett.* **2013**, *110*, 263901.
(108) Ciracì, C. Current-dependent potential for nonlocal absorption in quantum hydrodynamic theory. *Phys. Rev. B: Condens. Matter Mater. Phys.* **2017**, *95*, 245434.

DOI: 10.1021/acsphotonics.7b00538
ACS Photonics 2018, 5, 133−142